Preprint Title	Combining PVD structuration with dealloying for the creation of a highly efficient SERS platform
Authors	Adrien Chauvin, Walter Puglisi, Damien Thiry, Cristina Satriano, Rony Snyders and Carla Bittencourt
Publication Date	20 Sep 2022
Article Type	Full Research Paper
Supporting Information File 1	Electronic Supporting Information.pdf; 736.5 KB
ORCID® iDs	Adrien Chauvin - https://orcid.org/0000-0003-1896-8776; Cristina Satriano - https://orcid.org/0000-0001-5348-5863; Carla Bittencourt - https://orcid.org/0000-0002-3330-6693

Combining PVD structuration with dealloying for the creation of a highly efficient SERS platform

Adrien Chauvin,*[1,2] Walter Puglisi,[3] Damien Thiry,[1] Cristina Satriano,[3] Rony Snyders,[1,4] and Carla Bittencourt[1]

Address: [1]Plasma-Surface Interaction Chemistry, University of Mons, 23 Place du Parc, 7000 Mons, Belgium, [2]Chemistry of Surfaces, Interfaces and Nanomaterials, Faculty of Sciences, Université libre de Bruxelles, 50 Avenue F.D. Roosevelt, 1050 Brussels, Belgium, [3]Nano Hybrid BioInterfaces Lab (NHBIL), Department of Chemical Sciences, University of Catania, viale Andrea Doria, 6, 95125 Catania, Italy and [4]Materia Nova Research Center, 3 avenue Nicolas Copernic, 7000 Mons

Email: Adrien Chauvin - adrien.chauvin@umons.ac.be

* Corresponding author

Abstract

Nanostructured noble metal thin films are highly studied for their interesting plasmonic properties. The latter can be effectively used for the detection of small and highly diluted molecules by the surface-enhanced Raman scattering (SERS) effect. Regardless of impressive detection limits achieved, synthesis complexity and the high cost of gold restrict their use in devices. Here, we report on a novel two-step approach to design and fabricate efficient SERS platforms that combines the deposition of a silver-aluminum thin film with dealloying. The magnetron sputtering technique was used for the deposition of the alloy thin film to be dealloyed. After dealloying, the resulting silver nanoporous structures revealed two degrees of porosity: a macroporosity, associated to the initial alloy morphology and a nanoporosity, related to the dealloying step. The resulting nanoporous columnar structure was finely optimized by tuning the deposition (i.e., the alloy chemical composition) and dealloying (i.e., dealloying media) parameters to reach the best SERS properties. These are reported for the samples dealloyed in HCl and with 30 at.% of silver at the initial state with a detection limit down to 10^{-10} mol.L^{-1} for a solution of Rhodamine B.

Keywords

SERS; dealloying; nanoporous thin film; magnetron sputtering; nanostructuration

Introduction

Pollutant residues are strictly regulated in most countries to ensure water and food safety. In this context, there is an increasing demand for pollutant analysis tools with practical and cost-efficient methods. Compared to in-lab standard methods used for pollutant analysis (i.e., chromatography and mass spectrometry), Surface-enhanced Raman Scattering (SERS)-based sensors have emerged as serious candidates due to their rapidity, portability, and cost-effectiveness [1,2]. SERS sensors are promising for various applications in chemical (e.g. explosive [3] or chemical warfare agent [4]) or biological (e.g. lipid or protein [5]) sensing, environmental monitoring [6] as well as food safety through the detection of pollutants such as phenol [3,7], or rhodamine [8].

The SERS detection properties are mostly observed in noble metal nanoparticles [2]. Silver and gold are extensively utilized materials in the preparation of SERS substrates due to their localized surface plasmon resonance (LSPR) in the visible region [2,9]. Although the surface plasmon efficiency of Ag is higher than for Au, the susceptibility of Ag nanoparticles (NPs) to oxidation and its thermodynamical instability leading to morphology variation, result in the deterioration of their SERS efficiency [8]. Besides that, most studies report on the high SERS properties for NPs in suspension. However, NPs suspensions are hard to handle, suffer from poor stability, and can be hardly reused [6]. In this perspective, major interest has been devoted to develop solid SERS platforms made of nanostructured thin films [10]. Among them, nanoporous materials show superior properties due to their interconnected nanostructures and large surface areas [11,12]. A myriad of techniques is available for the synthesis of porous nanostructures [13,14]. Among them, dealloying has received particular attention due to its simple methodology [15]. The method

involves the leaching of the less noble component of an alloy creating a skeleton made of the noble element [16]. Dealloying is usually accomplished through a chemical step in which the alloy is dipped into an etching solution to remove the less noble metal [15]. This process leads to highly homogenous porous structure substrates with better reliability and stability, compared to conventional NP-based SERS substrates [17]. The race towards more efficient SERS platforms has led to the development of highly complex synthesis processes which limits their use in practical applications [18–21]. Most reports on efficient nanoporous platforms are based on gold, due to their high stability towards oxidation [22]. Therefore, heading towards simple and cheaper approaches to reach the industrial market turns out to be a necessity.

The origin of the SERS effect relies on the interaction between an intense electromagnetic field (EF) and the analyte through the i) electromagnetic enhancement and/or the ii) chemical enhancement [23]. Despite the impressive detection limit achieved by the nanoporous structures, little attention has been paid to the sample surface architecture, even if, among others, the SERS effect is highly dependent on the distance between nanostructures [24]. In fact, the electromagnetic enhancement, observed between two close NPs or in metallic nanotips, decays exponentially when the distance to the metal surface increases [23]. In other words, only analytes that are very close (i.e. less than 3 nm) to the surface, experience the EF [2]. Moreover, the chemical enhancement, occurs at an even shorter effective distance range since the molecules have to bond to the metal surface. Therefore, even though high EF enhancement can be achieved using SERS, the resulting signal intensity tends to vary strongly due to the surface contamination [24].

In this paper, a simple synthesis method to design bimodal porous silver substrate for SERS is reported. Magnetron co-sputtering of a silver and aluminum target was used for the deposition of the precursor alloy thin film. This approach allows

the synthesis of structured alloy thin films constituted of dispersed alloy columns. The dealloying of these films was implemented in three different media, i.e., HCl, H_3PO_4, and NaOH to highlight their impact on the SERS properties of the nanoporous structure. Using scanning electron microscopy (SEM) and X-Ray photoelectron spectroscopy (XPS) the morphology and the surface composition of each nanoporous structure were respectively evaluated and used to describe the SERS properties of the samples.

Results and Discussion

Morphology of Ag-Al alloy thin film

The deposition of the silver-aluminum thin films on silicon was accomplished by magnetron co-sputtering using a silver target and an aluminum one. To allow a good adhesion between silicon and the alloy thin film, a silver adhesion layer was deposited prior to the alloy thin film. Three different silver compositions were selected, namely 18, 30, and 36 at. % and characterized by SEM-EDX.

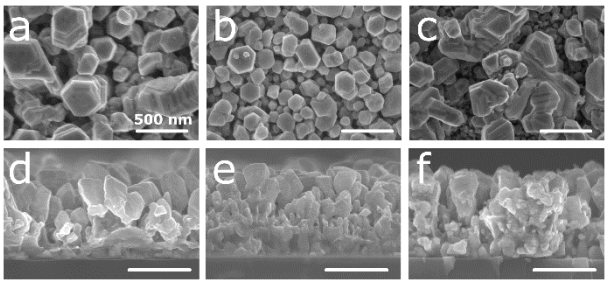

Figure 1: (a-c) Plan view and (d-f) cross section SEM images of the Ag-Al alloy thin film with an initial composition of (a and d) 18, (b and e) 30 and (c and f) 36 at. % Ag.

Figure 1 displays the SEM micrograph of the as-deposited thin films. The thin films exhibit a columnar morphology (see the cross-section SEM images in Figure 1d-f). The top view images (Figure 1a-c) reveal the presence of dispersed hexagonal columns with different dispersion and size. For the samples with 18 and 36 at. % of Ag (Figures 1a and c), the columns are larger and less packed than for the sample with 30 at. % of Ag (Figure b). Actually, the growth of islands has been observed for the deposition of silver alloys on silver [25]. Their growth mechanism relies on the Volmer-Weber (VW) growth mode that explains island growth. Briefly, the difference in wettability between the silver and the alloy leads to the preferential growth in the form of islands than in a homogenous film [26,27]. To support this assumption, the deposition was carried out for a short time (i.e. 2 min and 5 min, Figure S1) revealing the appearance of small islands at the early stage of the film growth confirming our explanation.

Optimization of the nanoporous structure

Influence of the initial Ag content and dealloying time

The nanoporous structure was tailored to obtain the best SERS efficiency for the detection of Rhodamine B (RhB). First, the influence of the dealloying time in the morphology was evaluated. Samples with 30 at. % of Ag were synthesized and the dealloying was performed in HCl during 10, 30, 60, and 120 min. The lamellar structure in the as-prepared sample is due to the rotation of the substrate during the deposition. The film presents a multilayer structure composed of Ag rich and Ag poor layers, which are formed because of the variation of distance between the rotating substrate and Ag target; Ag rich layers are formed when the substrate is close to the Ag target while Ag poor layer are formed when it is far. The formation of these nanolayer has already been reported in the literature [15,28].

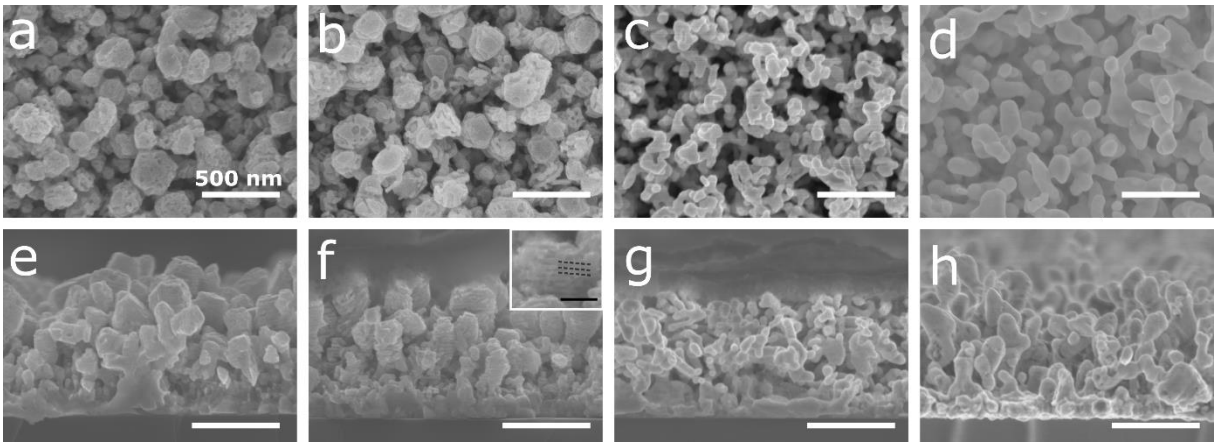

Figure 2: (a-d) Plan view and (e-h) cross section SEM images of the Ag-Al alloy thin film with an initial composition of 30 at. % Ag and dealloyed during (a and e) 10, (b and f) 30, (c and g) 60 and (d and h) 120 min in HCl solution at 1 wt.%. Scale bar: 500 nm. Inset of panel (f) corresponds to a magnification of a nanolayered structure, the dashed lines highlight a full layer. Scale bar 100 nm.

The SEM micrographs of the dealloyed thin films are shown in Figure 2. After 10 min in HCl, pores appear on the top of the Ag-Al thin film (Figure 2a) whereas no changes are observed in the cross-section images (Figure 2e). These small pores highlight the early dealloying stage and the propagating front at the grain boundaries [29]. For 30 min in HCl, bigger pores are formed (Figure 2b) and, the cross-section image shows structures made of a porous and full layers (Figure 2f). After 60 min of dealloying, the initial structure is hardly observed, and the creation of small ligaments is revealed through the film (Figure 2c and g). Finally, when reaching 120 min of dealloying, the material exhibits a nanoporous structure with larger ligaments than for 60 min of dealloying (Figure 2d and h). The increase of the ligament size corresponds to the late stage of dealloying characterized by a step of coalescence of the ligaments [29,30].

Next, the influence of the silver content in the Ag-Ag thin film on the dealloyed morphology was studied. For this purpose, the initial alloy composition was tuned at 18, 30, and 36 at. % of Ag. For sake of simplicity, the samples with 18, 30 and 36 at.% of Ag at initial state will be denoted AlAg18, AlAg30 and AlAg36, respectively. These concentrations were selected to avoid the passivation of the surface by silver as observed in our previous study (~50 at.%) [30].

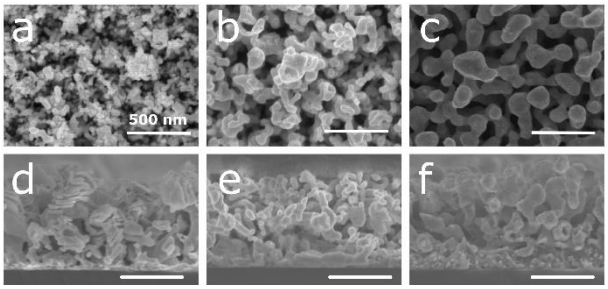

Figure 3: (a-c) Plan view and (d-f) cross section SEM images of the Ag-Al alloy thin film dealloyed during 60 min in HCl solution at 1 wt.% with an initial composition of (a, d) 18, (b, e) 30, and (c,f) 36 at.% of Ag. Scale bar: 500 nm.

On the SEM micrograph for the Ag-Al thin film dealloyed during 60 min in HCl (Figure 3a, b, and c), we observe an increase in the ligament size when increasing the initial Ag atomic content. Moreover, for the higher amount of initial Ag content (i.e. 30 and 36 at. %), the layered structure, noticed on the as-deposited samples, is not observed (Figure 3d,e,f). Thus, a decrease in the dealloying kinetics for higher amounts of silver at the initial state can be expected.

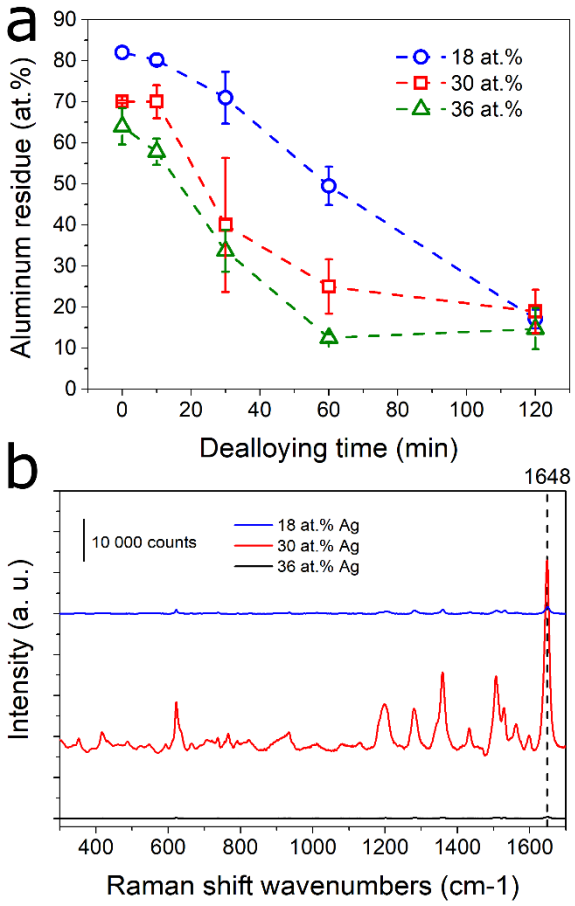

Figure 4: (a) Aluminium content evaluated by EDX for samples dealloyed in 1 wt. % HCl and for an initial Ag content of 18, 30 and 36 at. % in the film. (b) Raman spectra recorded after 24 h incubation in 10^{-7} mol·L^{-1} solution of RhB on nanoporous silver obtained after 60 min of dealloying in HCl solution with an initial composition of 18, 30 and 38 at.%.

The EDX analysis of the samples dealloyed in HCl confirms this hypothesis. Indeed, in Figure 4a it can be seen that the dealloying kinetics is faster for a higher amount of silver in the initial film with a faster decrease of aluminum content. However, this observation is not consistent with the previously reported studies on dealloying, revealing that the dealloying kinetics should be faster for samples with a lower amount of noble metals [15]. As previously shown for the case of the Ag-Al alloy dealloyed in HCl, the dealloying leads to the creation of a passivation layer, more pronounced for a

lower amount of Ag, which delays the dealloying [30]. This behavior can be seen for the sample AlAg30. The aluminum residue is stable after 10 min in an HCl solution and then drops to 25 at. % after 60 min in the etching solution. This behavior is associated to the creation of an AgCl passivation layer at the surface of the structure at the early stage of dealloying. When the passivation layer breaks down, then the HCl solution spreads quickly inside the structure and dissolves Al [31]. The large standard deviation of the composition after 30 min of dealloying suggests that the dealloying kinetic is different over the substrate. Due to the initial morphology, the passivation layer on every column will break down after different times in the HCl solution. The discrepancy of kinetics observed here compared to the literature can be explained by the confinement effect which slows down the dealloying in smaller pore since etching by-products stay trapped and limit further dealloying of the structure. In other words, the extraction of the $AlCl_3$, formed during the dealloying and confined in small pores is difficult since no solution agitation is applied making the dealloying kinetics slower. As highlighted by the SEM images (Figure 3), the pores are smaller for low amount of silver at initial content, thus by-products confinement effect is more likely to happen.

Then, we have studied the influence of the initial Ag content and the dealloying time on the SERS detection properties. To reach this objective, Raman spectra of the RhB diluted at 10^{-7} mol·L^{-1} were recorded on the samples after different dealloying time and for the three selected initial Ag content. As expected, no Raman signal was detected for the Ag-Al thin film before dealloying. As well, no Raman signal originating from RhB was detected for all the samples dealloyed for less than 60 min in HCl. The randomly organized small ligaments in the film and the rather high amount of aluminum residue didn’t allow the formation of effective ‘hot spots’ to enhance the Raman signal of RhB. Figure 4b shows the RhB Raman spectra collected on the samples dealloyed for 60 min. An intense Raman signal was recorded for the sample AlAg30 compared

to the other conditions. Then, the intensity of the RhB signal strongly decreased when samples dealloyed for longer times (i.e., 120 min, Figure S2) were used as SERS substrate. This behavior can be associated to the increase in the size of the ligaments which hinders the Raman signal of the RhB [32].

To understand the highest SERS performance of the AlAg30 sample dealloyed during 60 min, the composition of the surface of the film was probed by XPS. The SERS properties of a structure are driven by the presence of the 'hot spots'. These are highly sensitive to the composition of the surface since the presence of impurities can hinder the SERS properties [24]. The XPS composition of the surface of the samples dealloyed during 60 min in HCl and for the three selected Ag compositions is reported in Table 1.

Table 1: Surface composition evaluated by XPS of sample dealloyed during 60 min in 1 wt.% HCl for different initial Ag content.

Composition (at. %)	C	O	Al	Cl	Ag
18 at.% of initial Ag	12.0	58.4	22.4	0.2	7.0
30 at.% of initial Ag	9.1	28.5	1.9	6.5	54.0
36 at.% of initial Ag	17.8	35.8	10.7	0.9	34.8

As expected, the sample showing the best SERS efficiency is also the one with the highest concentration of Ag at the surface. Besides the presence of chlorine originating from the dealloying process, the analysis of the Ag 3d peak (Figure S3 and S4) reveals the presence of a loss peak indicating the metallic state of Ag. Therefore,

no AgCl complex is observed. Moreover, a shift is observed for the Ag 3d peak towards higher binding energy for sample with low initial Ag content. This shift is related to the smaller size of the ligaments at low Ag content as already reported for nanoparticles [33]. The lower SERS efficiency for samples AlAg18 and AlAg36 dealloyed 60 min can be associated to the presence of a higher carbon content at the surface. As already reported, the presence of carbon on a metal surface induces hydrophobicity which can also affect the bonding with RhB molecules [24].

Influence of the dealloying media

Finally, the influence of the dealloying media was studied. For this purpose, two other solutions were selected, i.e., H_3PO_4 and NaOH. Undoubtedly, anions play an important role during the dealloying process due to the intricate reaction between anions and Ag or Al [34,35]. More particularly, it has been reported that during dealloying in HCl, the Cl^- ion accelerates the diffusion of Ag atoms, and the Cl^- reaction with Al proceeds faster than for other anions [34]. To complete the optimization of the SERS nanoporous silver substrate towards the detection of RhB, the films with different silver compositions (i.e. 18, 30, and 36 at.%) were dealloyed using H_3PO_4 and NaOH. The SEM micrographs of the sample dealloyed during 60 min in H_3PO_4 and NaOH are shown in Figure S5 and S6. Despite the use of other dealloying media, the sample morphology is the same as for the one dealloying 60 min in HCl.

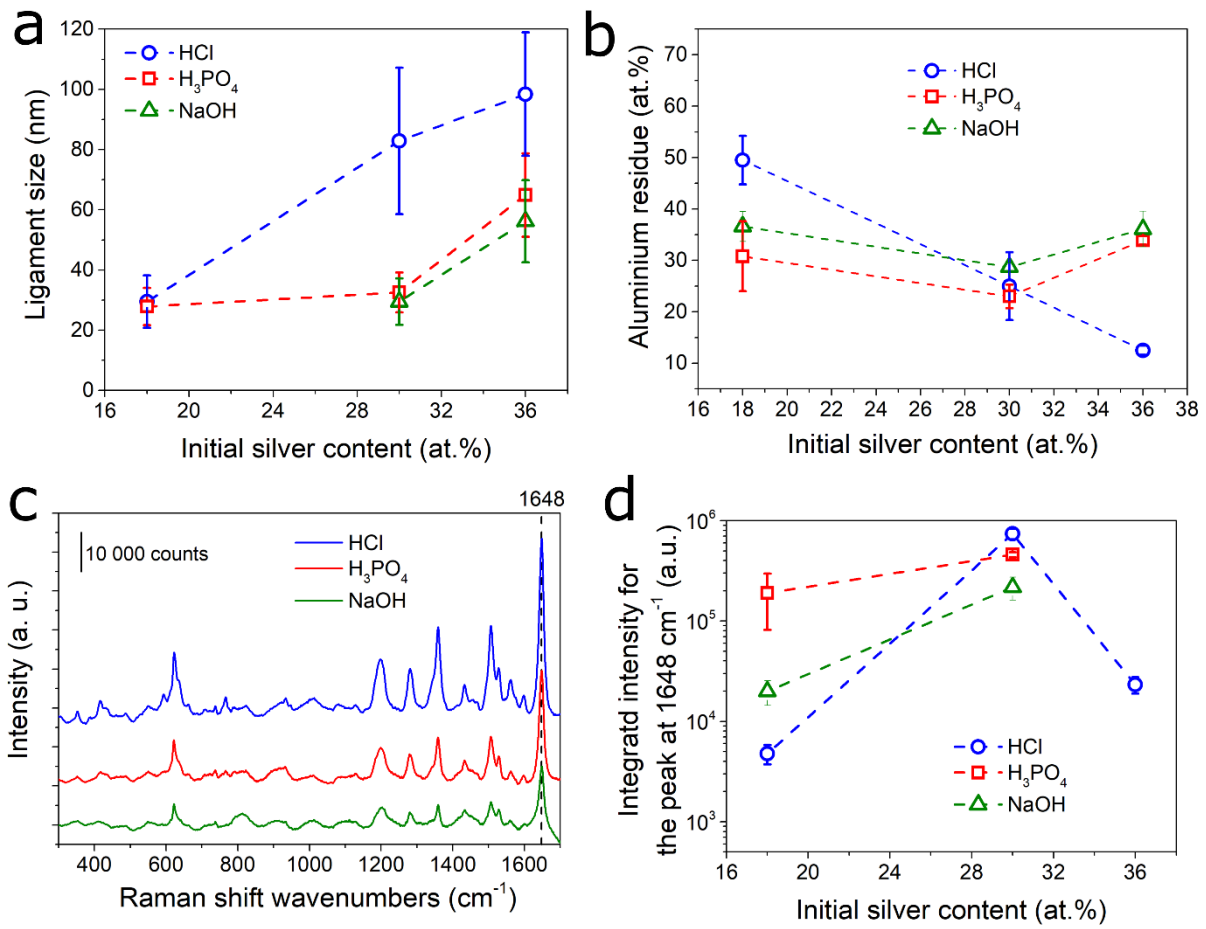

Figure 5: Evolution of the (a) ligament size and (b) the aluminium residue for sample dealloyed in HCl (blue), H_3PO_4 (red) and NaOH (green) for sample with different initial silver content at initial state. (c) Raman spectra recorded after 24 h incubation in 10^{-7} mol·L^{-1} RhB solution for Ag-Al samples with an initial amount of silver of 30 at. % and dealloyed for 60 min in (blue) HCl, (red) H_3PO_4 and (green) NaOH. (d) Comparison the integrated intensity of the peak at 1648 cm^{-1} for samples with different initial silver content and dealloyed in different solution incubated 24 h in 10^{-7} mol·L^{-1} RhB.

Figure 5a highlights the variation in the ligament size for the different initial silver content in the thin film and the different etching media. The ligament size increases when increasing the amount of initial silver in the film for the three dealloying media. For AlAg18, the ligament size is similar (around 30 nm) for all dealloying media, however for higher initial silver content, samples dealloyed in HCl reveal bigger

ligaments than the sample dealloyed in H_3PO_4 and NaOH. This observation can be related to the fast diffusion of the Ag promoted by the Cl^- ions [34]. Figure 5b displays the content of aluminum residue in the samples after dealloying probed by EDX. Two different behaviors can be observed: for the HCl media, the aluminum residue content decreases when increasing the initial silver content whereas for H_3PO_4 and NaOH, no change in the aluminum residue content is observed. For H_3PO_4 and NaOH, the dealloying proceeds at the same rate for all samples until the formation of a passivation layer containing silver which will protect the aluminum from further etching. Conversely, in the case of the dealloying in HCl, the reaction with silver led to the creation of an AgCl passivation layer protecting the aluminum etching, until the formation of soluble $[AgCl_2]^-$ complexes. The breakdown of the protective passivation layer will allow the etching of more quantities of aluminum compared to the dealloying in H_3PO_4 and NaOH [31]. Therefore, for a high amount of initial silver content in the thin film, the aluminum residue is lower for the sample dealloyed in HCl. On the other hand, the higher amount of aluminum residue after etching in HCl for the lowest amount of silver at the initial state might be due to the confinement effect discussed before. This affects the dealloying kinetics in a different way according to the initial silver content since smaller pores are observed for a lower amount of initial silver content. This effect is more pronounced for the samples dealloyed in HCl since the Cl^- ions accelerate the diffusion of the silver atoms and promote the dealloying [34]. After 120 min of dealloying, the aluminum residue drops to near 17 at.% for HCl and H_3PO_4 for the three different initial silver contents (Figure S7). For NaOH, the film completely delaminates after 120 min of dealloying, so the EDX analysis was not possible.

As mentioned previously, surface composition drives the SERS properties. Thus, the surface composition of the AlAg30 samples dealloyed 60 min in NaOH and H_3PO_4 was evaluated by XPS (Table 2).

Table 2: Surface composition evaluated by XPS of nanoporous silver thin films with 30 at. % of initial Ag content and dealloyed 60 min in different dealloying media.

Composition (at. %)	C	O	Al	Ag	P
30 wt.% NaOH	22.2	35.6	11.6	30.6	-
10 wt.% H_3PO_4	11.4	51.1	15.6	20	1.9

As for the sample dealloyed in HCl, the Ag 3d peak recorded on the sample dealloyed in H_3PO_4 reveals the presence of metallic silver at the surface of the nanoporous structure (Figure S8). Moreover, the presence 2 at. % of phosphorous coming from the etching solution can be noticed. The influence of the dealloying media on the SERS efficiency was probed for the detection of RhB (Figures 5c and d). The Raman spectra of the AlAg30 samples dealloyed in the different media are displayed in Figure 5c. The integrated intensity of the peak at 1648 cm^{-1} is highlighted in Figure 5d. For a low initial amount of silver (i.e. 18 at. %), besides a similar ligament size for all samples, the SERS efficiency are higher for H_3PO_4. This higher efficiency can be associated with the lowest amount of aluminum residue evaluated by EDX. Next best SERS efficiency is observed for the AlAg30 samples. Even though, independent of dealloying media, all samples have similar amount of aluminum residue, the best efficiency is reported for HCl. In this case, the chemical composition of the surface (i.e., high amount of silver and low amount of carbon) might explain the best SERS efficiency. Finally, for higher initial silver content (i.e. 36 at.%), no SERS signal was detected for samples dealloyed in H_3PO_4 and NaOH, and a drop of the intensity of the Raman signal was observed for samples dealloyed in HCl. The large ligaments

together with the high amount of carbon at the surface can explain the decrease or hinder in the SERS signal for samples with high silver content.

Detection limit

SERS-based sensors are mostly built to detect low concentration of molecules in a solution. Therefore, RhB solutions were diluted in order to reach the limit for which the signal of the molecule cannot be seen, corresponding to the limit of detection (LoD) of our material (Figure 6a).

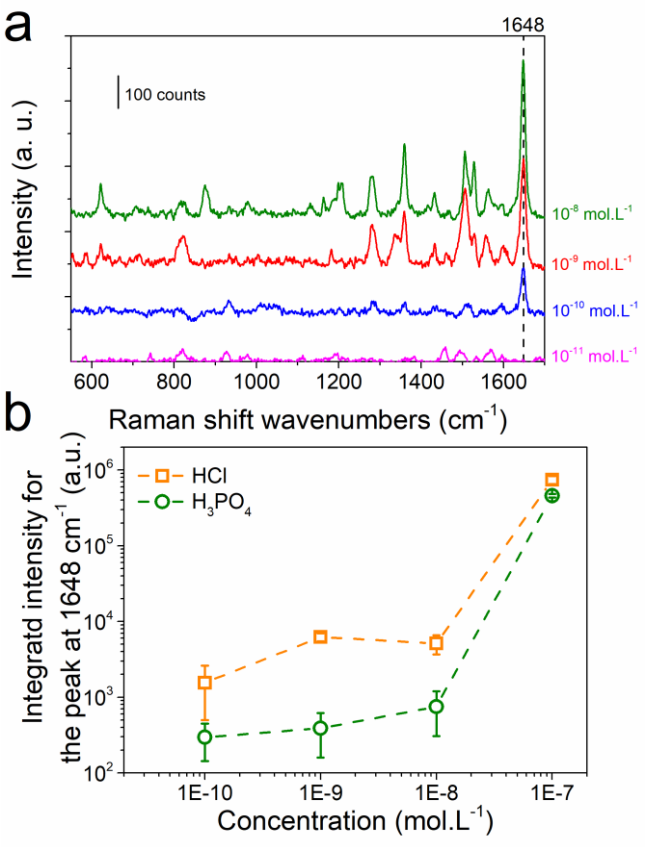

Figure 6: (a) Raman spectra recorded after 24 h incubation in RhB solution for different concentrations on a sample with an initial amount of silver of 30 at. % and dealloyed for 60 min in 1 wt. % of HCl. (b) Comparison of the evolution of the integrated peak at 1648 cm^{-1} for the different concentrations of RhB for samples with 30 at. % of silver at initial state and dealloyed for 60 min in (orange) 1 wt. % HCl and (green) 10 wt. % H_3PO_4.

For this part, AlAg30 thin films dealloyed during 60 minutes were selected since they present the higher Raman intensity of RhB at 10^{-7} mol·L^{-1} (Figure 6b). For sake of comparison, samples dealloyed in HCl and H_3PO_4 were analyzed. Figure 6a displayed the Raman spectra measured on the thin film dealloyed with HCl. The Raman signal of RhB strongly decreases when decreasing the RhB concentration from 10^{-7} mol·L^{-1} to 10^{-8} mol·L^{-1}. Then a plateau is observed until the complete vanishing of the Raman signal for RhB concentration of 10^{-11} mol·L^{-1}. Comparing the integrated intensity of the RhB peak, it can be observed that the intensity of the signal is lower for the sample dealloyed in H_3PO_4 than for the one dealloyed in HCl. Besides a lower intensity, the detection limit for both substrates is below 10^{-10} mol·L^{-1}. First, the LoD reported here is lower than the maximum allowable residue limit for RhB in food fixed by the European Union standard ($1.09 \cdot 10^{-9}$ mol·L^{-1}) [36]. Then, besides a lower LoD for RhB reported for complex nanostructure with grafted molecules (10^{-12} mol·L^{-1}) [37], or prepared from colloidal solution (10^{-13} mol·L^{-1}) [8,38], the approach reported here allows for an easy synthesis of a rather high sensible platform. Moreover, the reusability of the nanoporous silver structure for SERS detection has already been reported [1].

Conclusion

The development of an easy strategy to engineer efficient SERS platforms using nanoporous silver is reported for the detection of RhB. The synthesis approach relies on the structuration of an Ag-Al alloy thin film deposited by magnetron sputtering followed by dealloying. The structuration at the microscale was obtained by taking advantage of the difference in wettability of the silver and silver alloy to form dispersed

columnar thin films. The subsequent dealloying leads to a film structuration at the nanoscale range by the creation of porosity. The influence of three different dealloying solutions (i.e., NaOH, HCl, and H_3PO_4) on the SERS properties of the nanoporous structure is reported. Following the characterization of the surface, the structure and surface composition have been correlated with the SERS properties. Optimizing the thin film structuration, a limit of detection of 10^{-10} mol·L^{-1} is demonstrated. The high sensibility and the straightforward synthesis together with the ease to handle of this platform make it very promising for practical applications such as the detection of low concentrations of pollutants or biomolecules.

Experimental

Synthesis of the Ag-Al thin film

The Ag–Al thin films were deposited by DC magnetron co-sputtering in pure argon plasma of an Ag target (diameter: 50.8 mm; purity: 99.99%) and an Al (diameter: 50.8 mm; purity: 99.99%) target placed in a co-focal geometry. The distance between the targets and the substrate was 100 mm. The substrate was silicon. Prior to each deposition, a 50 nm Ag adhesion layer was grown by magnetron sputtering. While the power on the aluminum target was fixed to 150 W, the power on the silver target was tuned to 25, 50 and 75 W to create thin films with 18, 30 and 36 at. % of silver, respectively. The deposition was performed over a rotating of the substrate at 1.6 rpm. For all deposition the base pressure was less than 5.10^{-6} Torr, and the deposition pressure was fixed to $5{\cdot}10^{-3}$ Torr. The deposition time was fixed to 12 min to reach a thin film with a thickness of ~500 nm.

Dealloying of the Ag-Al thin film

The dealloying of the Ag-Al thin film was carried out in 1 wt.% hydrochloric acid (HCl), 30 wt.% sodium hydroxide (NaOH) and 10 wt.% phosphoric acid (H_3PO_4). The sample were immersed during the desired time and dipped in deionized water for 20 min to stop the dealloying and ensure a good cleaning of the sample.

Characterization

The scanning electron microscopy (SEM) micrograph were recorded using a HITACHI STEM-FEG with an acceleration voltage of 5 kV. The chemical composition of the films was determined by energy dispersive X-ray spectroscopy (EDX) with an acceleration voltage of 10kV. To evaluate the surface composition and oxidation state X-ray photoemission spectroscopy (XPS) was used. XPS measurements were carried out on a PHI 5000 VersaProbe using a monochromatic Al Kα X-ray source (1486.6 eV). The high-resolution spectra were recorded with a pass energy of 23 eV.

SERS measurements

Raman measurements were performed with a Senterra Bruker micro-Raman system spectrometer using a 533 nm excitation laser line with acquisition time of 10s. The power was fixed at 0.2 mW focused on the sample with a x50 objective. Rhodamine B (RhB) was chosen as SERS probe molecule. Prior to experiments, the porous silver was dipped in ultrapure water and dried. The sample were immersed during 24 hours in the ultrapure water solution containing the RhB with concentration varying from 10^{-7} to 10^{-11} mol·L^{-1}, enabling the molecule to be absorbed on the surface. This procedure was already used in our previous studies [6]. The sample were then dried in air prior to SERS measurements. Each analysis has been carried out on three different samples made in the same conditions and at three different areas for each

samples to get the standard deviation. In order to test the reproducibility of one surface, the analysis was performed in 9 different areas on the same sample, the RSD value for the integrated intensity is 16% (Figure S9).

Supporting Information

Supporting Information File 1:

File Name: Electronic Supporting Information

File Format: PDF

Title: Electronic Supporting Information for : Combining PVD structuration with dealloying for the creation of a highly efficient SERS platform

Acknowledgements

The authors gratefully acknowledge D. Cornelissen (Mons Univ.), Y. Paint (Materia Nova, Mons), D. Cossement (Materia Nova, Mons) and X. Noirfalise (Materia Nova, Mons) for their technical assistance on the cosputtering system, SEM , Raman and on the XPS, respectively. AC thanks the FNRS for the financial support through the “VirusSurf” project No H.P064.20. CB thanks the Belgian Fund for Scientific Research under the FRFC contract EQP 40002995 (PHOTOFUN). CB is a Research Associate of the National Funds for Scientific Research (FRS-FNRS).

References

(1) Chi, H.; Wang, C.; Wang, Z.; Zhu, H.; Mesias, V. St. D.; Dai, X.; Chen, Q.; Liu, W.; Huang, J. *Analyst* **2020**, *145*, 5158–5165. doi:10.1039/D0AN00999G

(2) Langer, J.; Jimenez de Aberasturi, D.; Aizpurua, J.; Alvarez-Puebla, R. A.; Auguié, B.; Baumberg, J. J.; Bazan, G. C.; Bell, S. E. J.; Boisen, A.; Brolo, A. G.; Choo, J.; Cialla-May, D.; Deckert, V.; Fabris, L.; Faulds, K.; García de Abajo, F. J.; Goodacre, R.; Graham, D.; Haes, A. J.; Haynes, C. L.; Huck, C.; Itoh, T.; Käll, M.; Kneipp, J.; Kotov, N. A.; Kuang, H.; Le Ru, E. C.; Lee, H. K.; Li, J.-F.; Ling,

X. Y.; Maier, S. A.; Mayerhöfer, T.; Moskovits, M.; Murakoshi, K.; Nam, J.-M.; Nie, S.; Ozaki, Y.; Pastoriza-Santos, I.; Perez-Juste, J.; Popp, J.; Pucci, A.; Reich, S.; Ren, B.; Schatz, G. C.; Shegai, T.; Schlücker, S.; Tay, L.-L.; Thomas, K. G.; Tian, Z.-Q.; Van Duyne, R. P.; Vo-Dinh, T.; Wang, Y.; Willets, K. A.; Xu, C.; Xu, H.; Xu, Y.; Yamamoto, Y. S.; Zhao, B.; Liz-Marzán, L. M. *ACS Nano* **2020**, *14*, 28–117. doi:10.1021/acsnano.9b04224

(3) Hu, X.; Wang, X.; Ge, Z.; Zhang, L.; Zhou, Y.; Li, J.; Bu, L.; Wu, H.; Li, P.; Xu, W. *Analyst* **2019**, *144*, 3861–3869. doi:10.1039/C9AN00251K

(4) Liyanage, T.; Rael, A.; Shaffer, S.; Zaidi, S.; Goodpaster, J. V.; Sardar, R. *Analyst* **2018**, *143*, 2012–2022. doi:10.1039/C8AN00008E

(5) Bruzas, I.; Lum, W.; Gorunmez, Z.; Sagle, L. *Analyst* **2018**, *143*, 3990–4008. doi:10.1039/C8AN00606G

(6) Chauvin, A.; Lafuente, M.; Mevellec, J. Y.; Mallada, R.; Humbert, B.; Pina, M. P.; Tessier, P.-Y.; El Mel, A. *Nanoscale* **2020**, *12*, 12602–12612. doi:10.1039/D0NR01721C

(7) Koklioti, M. A.; Bittencourt, C.; Noirfalise, X.; Saucedo-Orozco, I.; Quintana, M.; Tagmatarchis, N. *ACS Appl. Nano Mater.* **2018**, *1*, 3625–3635. doi:10.1021/acsanm.8b00747

(8) Ha Pham, T. T.; Dien, N. D.; Vu, X. H. *RSC Adv.* **2021**, *11*, 21475–21488. doi:10.1039/D1RA02576G

(9) Wu, C.; Huang, S.; Wang, Y.; Chai, Y.; Yuan, R.; Yang, X. *Anal. Chem.* **2021**, *93*, 11019–11024. doi:10.1021/acs.analchem.1c02336

(10) Camelio, S.; Babonneau, D.; Vandenhecke, E.; Louarn, G.; Humbert, B. *Nanoscale Adv.* **2021**, *3*, 6719–6727. doi:10.1039/D1NA00586C

(11) Wittstock, A.; Biener, J.; Erlebacher, J.; Bäumer, M. *Nanoporous Gold : From an Ancient Technology to a High-Tech Material*; Royal Society of Chemistry, 2012

(12) Cialone, M.; Celegato, F.; Scaglione, F.; Barrera, G.; Raj, D.; Coïsson, M.; Tiberto, P.; Rizzi, P. *Applied Surface Science* **2021**, *543*, 148759. doi:10.1016/j.apsusc.2020.148759

(13) El Mel, A.-A.; Stephant, N.; Hamon, J.; Thiry, D.; Chauvin, A.; Chettab, M.; Gautron, E.; Konstantinidis, S.; Granier, A.; Tessier, P.-Y. *Nanoscale* **2016**, *8*, 141–148. doi:10.1039/C5NR07145C

(14) El Mel, A.-A.; Chettab, M.; Gautron, E.; Chauvin, A.; Humbert, B.; Mevellec, J.-Y.; Delacote, C.; Thiry, D.; Stephant, N.; Ding, J.; Du, K.; Choi, C.-H.; Tessier, P.-Y. *The Journal of Physical Chemistry C* **2016**, *120*, 17652–17659. doi:10.1021/acs.jpcc.6b06393

(15) El Mel, A.-A.; Boukli-Hacene, F.; Molina-Luna, L.; Bouts, N.; Chauvin, A.; Thiry, D.; Gautron, E.; Gautier, N.; Tessier, P.-Y. *ACS Applied Materials & Interfaces* **2015**, *7*, 2310–2321. doi:10.1021/am5065816

(16) Erlebacher, J. *Journal of The Electrochemical Society* **2004**, *151*, C614. doi:10.1149/1.1784820

(17) Chen, L.-Y.; Yu, J.-S.; Fujita, T.; Chen, M.-W. *Advanced Functional Materials* **2009**, *19*, 1221–1226. doi:10.1002/adfm.200801239

(18) Zhang, L.; Liu, H.; Chen, L.; Guan, P.; Chen, B.; Fujita, T.; Yamaguchi, Y.; Iwasaki, H.; Xue, Q.-K.; Chen, M. *RSC Advances* **2016**, *6*, 2882–2887. doi:10.1039/C5RA22321K

(19) Zhang, T.; Sun, Y.; Hang, L.; Li, H.; Liu, G.; Zhang, X.; Lyu, X.; Cai, W.; Li, Y. *ACS Applied Materials & Interfaces* **2018**, *10*, 9792–9801. doi:10.1021/acsami.7b17461

(20) Rajput, A.; Kumar, S.; P. Singh, J. *Analyst* **2017**, *142*, 3959–3966. doi:10.1039/C7AN00851A

(21) Jonker, D.; Jafari, Z.; Winczewski, J. P.; Eyovge, C.; Berenschot, J. W.; Tas, N. R.; Gardeniers, J. G. E.; De Leon, I.; Susarrey-Arce, A. *Nanoscale Adv.* **2021**, *3*, 4926–4939. doi:10.1039/D1NA00316J
(22) Huang, J.; Tang, C.; Chen, G.; He, Z.; Wang, T.; He, X.; Yi, T.; Liu, Y.; Zhang, L.; Du, K. *ACS Appl. Mater. Interfaces* **2021**, *13*, 7735–7744. doi:10.1021/acsami.0c20766
(23) Kneipp, K.; Moskovits, M.; Kneipp, H. *Surface Enhanced Raman Scattering: Physics and Applications*; Springer, 2006
(24) Matikainen, A.; Nuutinen, T.; Itkonen, T.; Heinilehto, S.; Puustinen, J.; Hiltunen, J.; Lappalainen, J.; Karioja, P.; Vahimaa, P. *Sci Rep* **2016**, *6*, 37192. doi:10.1038/srep37192
(25) Dutheil, P.; Thomann, A. L.; Lecas, T.; Brault, P.; Vayer, M. *Applied Surface Science* **2015**, *347*, 101–108. doi:10.1016/j.apsusc.2015.04.052
(26) Sarakinos, K. *Thin Solid Films* **2019**, *688*, 137312. doi:10.1016/j.tsf.2019.05.031
(27) Kaiser, N. *Applied Optics* **2002**, *41*, 3053. doi:10.1364/AO.41.003053
(28) Chauvin, A.; Horak, L.; Duverger-Nédellec, E.; Dopita, M.; Tessier, P.-Y.; El Mel, A.-A. *Surface and Coatings Technology* **2020**, *383*, 125220. doi:10.1016/j.surfcoat.2019.125220
(29) Niauzorau, S.; Sharstniou, A.; Sampath, V. K.; Kublik, N.; Bandarenka, H.; Azeredo, B. *ACS Appl. Mater. Interfaces* **2022**, *14*, 17927–17939. doi:10.1021/acsami.1c24388
(30) Chauvin, A.; Txia Cha Heu, W.; Tessier, P.-Y.; El Mel, A.-A. *physica status solidi (b)* **2016**, *253*, 2167–2174. doi:10.1002/pssb.201600604
(31) Wang, X.; Qi, Z.; Zhao, C.; Wang, W.; Zhang, Z. *The Journal of Physical Chemistry C* **2009**, *113*, 13139–13150. doi:10.1021/jp902490u
(32) Qian, L. H.; Yan, X. Q.; Fujita, T.; Inoue, A.; Chen, M. W. *Applied Physics Letters* **2007**, *90*, 153120. doi:10.1063/1.2722199
(33) Bittencourt, C.; Hecq, M.; Felten, A.; Pireaux, J. J.; Ghijsen, J.; Felicissimo, M. P.; Rudolf, P.; Drube, W.; Ke, X.; Van Tendeloo, G. *Chemical Physics Letters* **2008**, *462*, 260–264. doi:10.1016/j.cplett.2008.07.082
(34) Song, T.; Gao, Y.; Zhang, Z.; Zhai, Q. *CrystEngComm* **2011**, *13*, 7058. doi:10.1039/c1ce05538k
(35) Qiu, H.; Zhang, Z.; Huang, X.; Qu, Y. *ChemPhysChem* **2011**, *12*, 2118–2123. doi:10.1002/cphc.201100205
(36) Wu, N.; Gao, W.; Lian, Y.; Du, J.; Tie, X. *Food Chemistry* **2017**, *237*, 786–792. doi:10.1016/j.foodchem.2017.05.147
(37) Fang, C.; Agarwal, A.; Buddharaju, K. D.; Khalid, N. M.; Salim, S. M.; Widjaja, E.; Garland, M. V.; Balasubramanian, N.; Kwong, D.-L. *Biosensors and Bioelectronics* **2008**, *24*, 216–221. doi:10.1016/j.bios.2008.03.032
(38) Ashok Kumar, E.; Jiann Wang, T.-; Chang, Y.-H. *Applied Surface Science* **2022**, *585*, 152696. doi:10.1016/j.apsusc.2022.152696